

Harvesting the electromagnetic energy confined close to a hot body

Philippe Ben-Abdallah¹ and Svend-Age Biehs²

¹ *Laboratoire Charles Fabry, UMR 8501, Institut d'Optique, CNRS, Université Paris-Sud 11, 2, Avenue Augustin Fresnel, 91127 Palaiseau Cedex, France and*

² *Institut für Physik, Carl von Ossietzky Universität, D-26111 Oldenburg, Germany*

(Dated: November 18, 2021)

In the close vicinity of a hot body, at distances smaller than the thermal wavelength, a high electromagnetic energy density exists due to the presence of evanescent fields radiated by the partial charges in motion around its surface. This energy density can surpass the energy density in vacuum by several orders of magnitude. By approaching a PV cell with a band gap in the infrared frequency range this non-radiative energy can be transferred to it by photon tunneling and surface mode coupling. Here we review the basic ideas and recent progress in near-field energy harvesting.

I. INTRODUCTION

Thermophotovoltaic devices [1, 2] are energy conversion systems that generate electric power directly from thermal radiation. While in classical photovoltaic conversion devices the efficiency (defined as the ratio of the electric power produced by the cell over the net radiative power exchanged between the primary source and the cell) is bounded by the thermodynamic Shockley-Queisser limit [3] (30% for cells with a gap energy $E_g = 1$ eV and 10% for $E_g = 0.5$ eV), with near-field thermophotovoltaic (NTPV) systems this limit can, in principle, be surpassed by exploiting the strong heat transfer due to tunneling of non-propagating photons. In particular, with a quasi-monochromatic source, as those made with materials which support a surface wave, the efficiency can be close to one when this frequency coincides with the gap frequency of semiconductor [4]. Moreover, the strong magnitude of exchanges in plane-plane geometry [5] in near-field regime compared with what happens in far-field regime (which cannot exceed the black-body limit [6]) can lead to a generated power between 1 W cm^{-2} and 120 W cm^{-2} in the temperature range 500K-1200K for separation distances between the source and the cell of 10nm [7]. As a result a cell of 25cm^2 could theoretically generate a power of 25W-3000W. This is a very large value. The typical energy demand of a household in US [8] is 2500W, for instance.

In this paper we describe the basic principles behind this near-field technology and we briefly discuss the main issues which limit to date its massive deployment.

II. ELECTROMAGNETIC ENERGY CLOSE TO A HOT BODY

It is well known that the spectral energy density of thermal radiation at a given equilibrium temperature T follows the Planck law

$$u_{\text{BB},\omega} = \Theta(T)D_{\text{vac}}(\omega) \quad (1)$$

where

$$\Theta(T) = \frac{\hbar\omega}{e^{\hbar\omega/k_{\text{B}}T} - 1} \quad (2)$$

is the mean energy of a harmonic oscillator in thermal equilibrium and

$$D_{\text{vac}}(\omega) = \frac{\omega^2}{\pi^2 c^3} \quad (3)$$

is the density of states in vacuum. Here, we have introduced the Boltzmann constant k_{B} , the reduced Planck constant \hbar , and the light velocity in vacuum c . The maximum of the Planck spectrum is at a frequency of $\omega_{\text{th}} = 2.82\omega_c$ with $\omega_c = k_{\text{B}}T/\hbar$. As function of wavelength the maximum is at the thermal wavelength λ_{th} given by Wien's displacement law $\lambda_{\text{th}} = 2897\mu\text{m K}/T$, i.e. at 300 K the dominant frequency is $\omega_{\text{th}} \approx 10^{14}$ rad/s and the dominant wavelength $\lambda_{\text{th}} \approx 10 \mu\text{m}$.

Now, close to a thermal emitter at distances smaller than the thermal wavelength λ_{th} the properties of the emitter itself enter into the density of states and therefore also into Planck's law. Close to a thermal emitter as sketched in Fig. 1 in the particular case of a hexagonal boron nitride (hBN) sample a generalized Planck law can be derived which has the form [9–11]

$$u_{\omega} = \Theta(T)D_{\text{loc}}(\omega) \quad (4)$$

where $D_{\text{loc}}(\omega)$ is the local density of states. It depends in general on the geometry and optical properties of the emitter and on the position with respect to the emitter at which it is evaluated. For an emitter with a planar interface due to the translation symmetry with respect to planes parallel to the interface it depends on the distance z and the properties of the emitter. It can be shown that for $z \gg \lambda_{\text{th}}$ it converges to the density of states in vacuum $D_{\text{loc}} \rightarrow D_{\text{vac}}$ and in the opposite quasi-static regime for $z \ll \lambda_{\text{th}}$ it becomes larger than the vacuum density of states and diverges like $D_{\text{loc}} \propto 1/z^3$. Therefore, the energy density of thermal radiation close to a hot body is in general distance dependent and its magnitude can be larger than that predicted by Planck's law. This can be attributed to the contribution of evanescent waves existing in the vicinity of the emitter which have electromagnetic fields which are exponentially decaying with respect to the emitters interface. Such waves are for example total internal reflection waves and surface waves. As was already shown by Eckhardt [10] and later studied in detail by Shchegrov *et al.* and Joulain *et al.* [12, 13] the

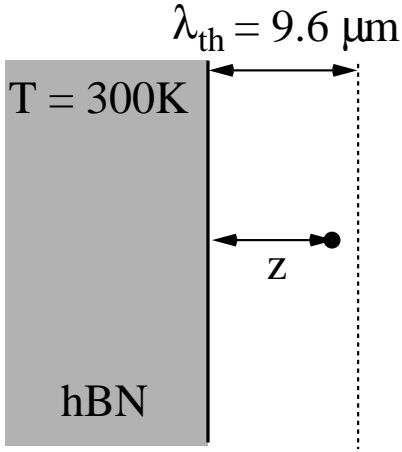


Figure 1: Sketch of the planar sample in global equilibrium at temperature $T = 300$ K. The energy density at a near-field distance $z < \lambda_{\text{th}} = 9.6 \mu\text{m}$ highly depends on the properties of the thermal emitter which is here hBN.

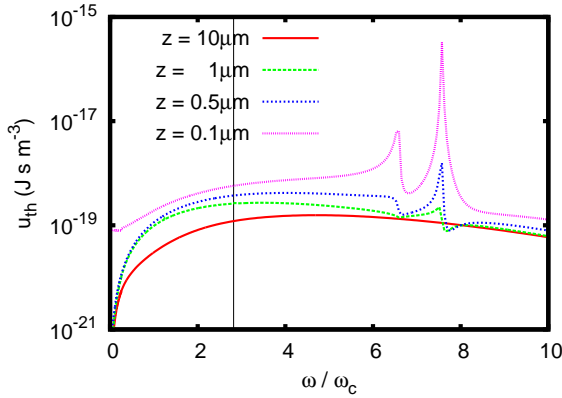


Figure 2: Semi-log plot of the spectral energy density u_ω in a distance z above a hBN halfspace at $T = 300$ K. The thermal wavelength is therefore $10 \mu\text{m}$. Therefore the spectrum at $z = 10 \mu\text{m}$ coincides mainly with the blackbody spectrum $u_{\text{BB},\omega}$. The vertical line is at the maximum frequency of the blackbody spectrum at $2.82\omega_c$ with $\omega_c = 3.5 \times 10^{13}$ rad/s. For more details see Refs. [11–13].

surface waves can lead to an extremely enhanced quasi-monochromatic near-field energy density spectrum. In metals such surface waves are surface-plasmon polaritons and in polar dielectrics such surface waves are known as surface-phonon polaritons (SPhP).

In Fig. 2 we show the energy density close to a hBN emitter. The optical phononic properties of hBN is described by the Drude-Lorentz model [14]

$$\epsilon_e(\omega) = \epsilon_\infty \frac{\omega^2 - \omega_L^2 + i\gamma\omega}{\omega^2 - \omega_R^2 + i\gamma\omega}, \quad (5)$$

with $\epsilon_\infty = 4.88$, $\omega_L = 3.032 \times 10^{14}$ rad/s, $\omega_R = 2.575 \times 10^{14}$ rad/s and $\gamma = 1.001 \times 10^{12}$ rad/s. As shown in Fig. 2 for hBN which supports surface-phonon polari-

tons the spectral energy density becomes dominated by the surface-phonon-polariton resonance at the frequency ω_{sp} for very small distances $z \ll \lambda_{\text{th}}$. This resonance frequency is in general for surface modes on planar interfaces implicitly defined by the condition $\text{Re}(\epsilon(\omega_{sp})) = -1$ where ϵ is the complex permittivity of the emitter which here has an interface with the vacuum. For metals the surface mode resonances are typically in the UV region and for polar dielectrics they are in the infrared. In particular, for hBN the resonance frequency is $\omega_{sp} = 2.960 \times 10^{14}$ rad/s which corresponds to a wavelength of $5 \mu\text{m}$. Hence the resonance is very close to the thermal wavelength λ_{th} at 300 K and can therefore be thermally excited at room temperature which is not the case for the surface waves in metals. Note, that the thermal near-field energy density can be tuned by texturing the material or by depositing 2D sheets on its surface [22, 23] and it is accessible with different scanning probe devices [15–21].

III. NEAR-FIELD HEAT TRANSFER

When bringing a receiver with temperature T_r close to an emitter at higher temperature $T_e > T_r$ as sketched in Fig. 3 then in general the propagating and evanescent waves generated by the thermal motion of the charges inside the emitter and receiver will contribute to the heat transfer. It has already been shown in the 1970's that when the receiver enters the near-field regime of the emitter, i.e. for emitter-receiver distances $d < \lambda_{\text{th}}$ then the resulting radiative heat flux Φ can in this case become much larger than the blackbody value due to the contribution of the evanescent waves which are confined at the surface of the emitter when the distance becomes smaller than the dominant thermal wavelength [5, 24–26]. About thirty years later, the idea to exploit the huge energy density of the evanescent waves for energy harvesting was brought forward by replacing the receiver by a photovoltaic cell [27–30]. In Ref. [28] a first detailed study of NTPV cells based on the framework of fluctuational electrodynamics [31] is provided. A first experimental proof of concept was provided by DiMatteo *et al.* [32]. These works paved the way for a large number of mainly theoretical works on near-field thermo-photovoltaics.

The theoretical foundation is the general expression for the heat flux between two materials with planar interfaces which was first determined within the framework of fluctuational electrodynamics [31] by Polder and van Hove [5]. This expression can be cast into a Landauer-like form by [33, 34]

$$\Phi(d) = \int_0^\infty \frac{d\omega}{2\pi} \Delta\Theta(\omega) \sum_{j=s,p} \int \frac{d^2\mathbf{k}_\perp}{(2\pi)^2} \mathcal{T}_j(\omega, \mathbf{k}_\perp; d) \quad (6)$$

where

$$\Delta\Theta(\omega) = \Theta(T_e) - \Theta(T_r) \quad (7)$$

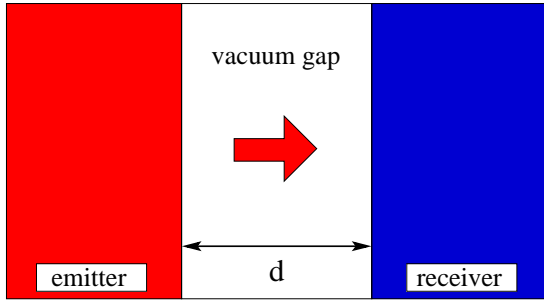


Figure 3: Sketch of the emitter and receiver separated by a vacuum gap of thickness d . In NTPV the receiver is replaced by a low band-gap photovoltaic cell.

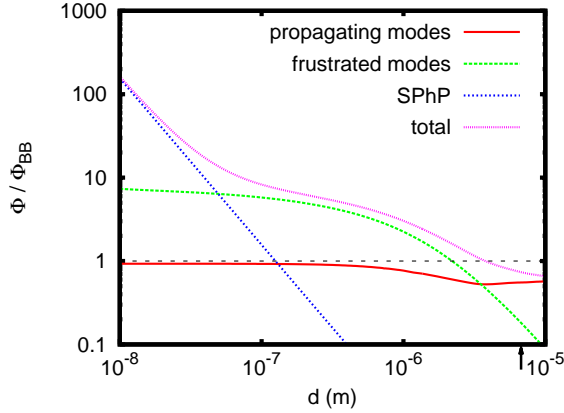


Figure 4: Near-field heat flux Φ between two hBN half-spaces normalized to the blackbody value Φ_{BB} as function of distance d . Here the temperature of the emitter is 300K and the temperature of the receiver is 0K so that $\Phi_{BB} = 459.27 \text{ Wm}^{-2} = 0.046 \text{ Wcm}^{-2}$. The contribution of different modes to the near-field heat flux is highlighted. For more details see Ref. [35].

and $\mathcal{T}_j(\omega, \mathbf{k}_\perp; d) \in [0 : 1]$ is the transmission factor for a given transversal mode with lateral wave vector $\mathbf{k}_\perp = (k_x, k_y)^t$, frequency ω and polarisation j (s - TE polarisation; p - TM polarisation). The transmission factor $\mathcal{T}_j(\omega, \mathbf{k}_\perp; d)$ is fully determined by the optical properties of the receiver and emitter. The contributions of the propagating waves are restricted to waves with wavevectors $|\mathbf{k}_\perp| \leq k_0$ and the evanescent wave contributions stem from waves with wavevectors $|\mathbf{k}_\perp| > k_0$.

It is clear that the maximum contribution of the propagating waves is obtained by setting $\mathcal{T}_j \equiv 1$ for all $|\mathbf{k}_\perp| \leq k_0$. Then the above expression gives the blackbody result

$$\Phi_{BB} = \sigma_{BB} [T_e^4 - T_r^4] \quad (8)$$

where $\sigma_{BB} = 5.67 \times 10^{-8} \text{ Wm}^{-2} \text{ T}^{-4}$ is the Stefan-Boltzmann constant. As a consequence it becomes apparent that the contribution of the evanescent waves will add to the heat flux of the propagating waves and therefore it can be larger than Φ_{BB} . In Fig. 4 the contributions

of the different heat flux channels for two hBN plates is highlighted. It can be seen that the propagating modes dominate in the far-field regime with $d > \lambda_{th}$ whereas the evanescent modes dominate in the near-field regime with $d < \lambda_{th}$. The near-field regime can be divided into the regime $d < \lambda_{th}/10$ where the surface modes dominate and the intermediate regime with $\lambda_{th}/10 < d < \lambda_{th}$ where the frustrated modes dominate [35–37]. The behaviour observed Fig. 4 is similar for other materials like SiC, silica or sapphire supporting surface modes in the infrared. For example, for SiC with a surface mode resonance at $\omega_{sp} = 1.787 \times 10^{14} \text{ rad/s}$ the enhancement would be $1000\Phi_{BB}$ at $d = 10 \text{ nm}$ for the choice of temperatures in Fig. 4 and for silica even higher enhancement factors are achievable. Depending on the shape and temperature regimes optimized material parameters can be obtained to increase the energy density and the heat flux [38–40].

First measurements of the near-field heat transfer between two planar samples were already conducted in the 1970's by Hargreaves and Domoto *et al.* [41–43] for metallic samples. A new era of near-field measurements has been started with the seminal work of Ottens *et al.* in 2011 [44] who could measure the heat flux between macroscopic 50mm x 50mm sapphire plates, which support surface modes in the infrared, down to a distance of about 2 micrometers. The aspect ratio between the smallest interplate distance to the lateral extension of the samples is approximately 1:25000. The measured enhancement was found to be 1.26 times the blackbody value [44] and can be attributed to the contribution of the frustrated total reflection modes. The following works have improved the experimental techniques in order to reduce the interplate distances as much as possible and to achieve the highest possible near-field enhancement [44–57]. State-of-the-art setups like the experiment by Reddy's group in Ref. [57] are now capable of measuring the heat flux between a $50 \mu\text{m} \times 50 \mu\text{m}$ silica emitter and an extended silica receiver down to 25nm and found an enhancement of about 700 times the blackbody value proving the possibility to have extremely large radiative heat fluxes due to the surface mode interaction in silica. Note that in most recent experimental setups the smaller distances are achieved by reducing the size of the samples so that for example the aspect ratio in the experiment [57] is 1:2000.

One of the technical challenges for near-field thermophotovoltaics will be to use the near-field effect for large scale PV cells. To achieve this goal several structures using different kind of spacers having a small heat conductivity were proposed [45, 50, 53, 54]. The spacers make it possible to keep the emitter and receiver in a controlled near-field distance. For example, Ito *et al.* measured in such a structure the radiative heat flux between two 19mm x 8.6mm quartz plates with microstructured pillars down to 500nm [50], i.e. the aspect ratio is in this case about 1:17200. One of the drawbacks of such a solution is that the heat conduction through the pillars is relatively large. Consequently by this conduction the receiver will heat up which will reduce the efficiency of any near-field

thermophotovoltaic device. In the setup of Ito *et al.* the heat flux through the spacers was on the same order of magnitude as the radiative heat flux between the emitter and the receiver. The goal of future setups or devices using spacers is therefore clearly to reduce this contribution of heat conduction through the spacers while having large areas for thermal radiation and a high stability.

IV. NEAR-FIELD ENERGY CONVERSION

As demonstrated in the previous sections the radiative heat flux by the surface-phonon-polariton contribution can be extremely large and as the surface-phonon-polariton contribution to the energy density it can also be quasi-monochromatic. This is a promising feature for an exploitation in near-field thermophotovoltaic devices. It has been shown in a theoretical study by Narayanaswamy and Chen in 2001 [58] that the surface modes of phonon-polaritonic emitters like SiC, cubic and hexagonal boron nitride will result in a tremendous increase of the heat flux into a direct band gap PV cell. A first quantitative calculation of the photocurrent and electric power in a tungsten-GaSb configuration was provided by Laroche *et al.* [4] assuming 100% quantum efficiency of the PV cell, i.e. it is assumed that all the incoming or absorbed heat radiation will be converted into a photocurrent. It could be shown that the conversion efficiency converges in this case towards 29% for distances below 100nm. Theoretically a generated electric power output of $3 \times 10^4 \text{ Wm}^{-2}$ was reported for a distance of 5nm. It should be noted that the Shockley-Queisser limit for a blackbody illuminating a GaSb cell is an efficiency of 29%. It was theoretically demonstrated that a quasi-monochromatic emitter like those considered by Narayanaswamy and Chen [58] can even beat the Shockley-Queisser limit in the near-field regime yielding 35% at an extremely small distance of 5nm which can be hardly achieved in real NTPV devices.

To illustrate the potential of the NTPV technology for energy harvesting we consider a system composed by a hot emitter made of hexagonal Boron Nitride (hBN) at temperature T_e placed in the proximity of a junction cell at temperature $T_r < T_e$ made of Indium Antimonide (InSb) with a gap frequency $\omega_g = 1.8231 \times 10^{14} \text{ rad/s}$ ($E_g = 0.12 \text{ eV}$). We use the optical properties of hBN from Eq. (5) and the dielectric function of the PN junction defined as [59]

$$\epsilon_r(\omega) = \begin{cases} n_r^2(\omega), & \omega < \omega_g, \\ (n_r(\omega) + in_i(\omega))^2, & \omega > \omega_g, \end{cases} \quad (9)$$

where

$$n_r = \sum_{j=1}^4 \frac{B_j \omega + C_j}{\omega^2 - B_j \omega + C_j} \quad (10)$$

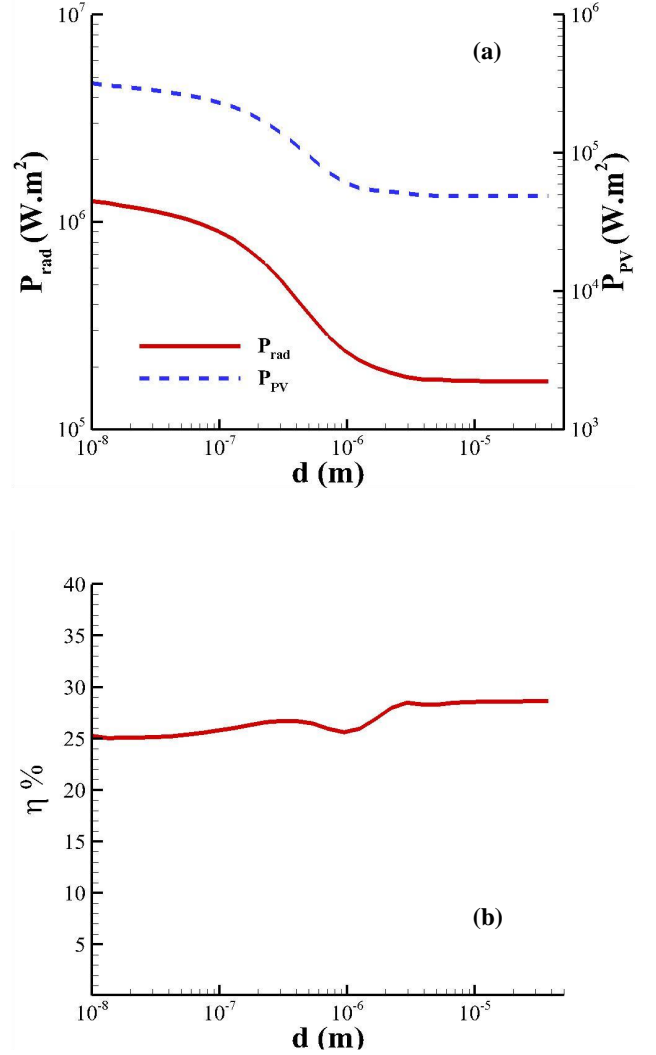


Figure 5: (a) Radiative power exchanged between a hBN thermal source at $T_e = 1500 \text{ K}$ and a InSb junction at $T_s = 300 \text{ K}$ and electric power generated in this system with respect to the separation distance. (b) Efficiency of produced electricity in a hBN/InSb TPV conversion system with respect to the separation distance between the source and the cell.

and

$$n_i = \frac{\alpha_0 c}{2\omega} \sqrt{\frac{\omega}{\omega_g} - 1} \quad (11)$$

with $B_j = \frac{a_j}{q_j}(E_g b_j - \frac{1}{2} b_j^2 - E_g^2 + c_j)$, $C_j = \frac{a_j}{q_j}((E_g^2 + c_j) \frac{b_j^2}{2} - 2E_g c_j)$ and $q_j = \frac{1}{2} \sqrt{4c_j - b_j^2}$. The constants a_j , b_j and c_j ($j = 1 - 4$) are tabulated values and depend on the type of semiconductors [59]. It is direct to verify that hBN supports a surface phonon-polariton resonance at frequency $\omega_{\text{spp}} \simeq 2.960 \times 10^{14} \text{ rad s}^{-1}$, larger than ω_g as desired.

The radiative power exchanged between the source and the junction reads

$$P_{\text{rad}} = \int_0^\infty \frac{d\omega}{2\pi} K(\omega) [\Theta(\omega, T_e) - \Theta(\omega - \omega_0, T_r)] H(\omega - \omega_g). \quad (12)$$

where H denotes the Heaviside function, $\omega_0 = eV_0/\hbar$. V_0 being the potential difference at which the cell is operating and which is here [61] taken as $\hbar\omega_g(1 - T_r/T_e)/e$ introducing the elementary charge e . The quantity

$$K(\omega) = \sum_{j=\{\text{s,p}\}} \int \frac{d^2\mathbf{k}_\perp}{(2\pi)^2} \mathcal{T}_j(\omega, \mathbf{k}_\perp; d) \quad (13)$$

is the number of modes per unit area which contribute to the transfer weighted by the Landauer transmission probability $\mathcal{T}_j(\omega, k)$ between the source and the cell in polarization j of the energy $\hbar\omega$ carried by the mode $(\omega, \mathbf{k}_\perp)$. The two terms in expression (12) represent the emission radiated by the source toward the cell and the power radiated back from the cell in direction of the source, respectively. As for the electric power density which is generated in the cell, it reads

$$P_{\text{PV}} = eV_0 \int_{\omega_g}^\infty \frac{d\omega}{2\pi} [\Theta(\omega, T_e) - \Theta(\omega - \omega_0, T_r)] \frac{K(\omega)}{\hbar\omega} \quad (14)$$

assuming a quantum efficiency of 100%. In Figure 5 we show the evolution of the power transferred to the cell and the electric power generated by the system with respect to the separation distance d between the source and the cell. We also plot in Fig. 5(b) the efficiency $\eta = P_{\text{PV}}/P_{\text{rad}}$ of the cell. For separation distances larger than the thermal wavelength λ_{th} the power exchanged between the source and the cell is mainly due to propagating photons so that it is independent on the distance. At subwavelength distances the radiative heat exchanges increase as the separation distance decays. This enhancement of exchanges is directly related to the number of contributing modes with respect to the separation distance [33, 34]. As discussed in the previous section at subwavelength distance the non-propagating modes (i.e. evanescent modes) superimpose to the propagating ones giving rise to new channels for heat exchanges by photon tunneling between the source and the cell. As a direct consequence these photons can generate further electron-hole pairs inside the junction and therefore increase the production of electricity. Hence at $d = 500\text{nm}$ the generated power is doubled compared to what happens in far-field regime. In extreme near-field regime this power is almost an order of magnitude larger than in far-field. As the efficiency is concerned we see in Fig.5(b) that in near-field the efficiency is a bit reduced in comparison with the performances of TPV conversion device in far-field regime. Nevertheless we have in this case an efficiency of about 25% and the output power at a realistic distance of 100nm is approximately 220kWm^{-2} .

Note that while the surface phonon-polariton of hBN is located at $5\mu\text{m}$ the gap of InSb cell is around $7.3\mu\text{m}$. This spectral mismatch reduces the conversion performances. By adding a sheet of graphene to the emitter or receiver, the heat flux by the surface modes and hence the efficiency can be increased in the extreme near-field regime [7, 61, 62]. In Ref. [7] an efficiency of 30% (40%) with a generated power of 6Wcm^{-2} (120Wcm^{-2}) was reported for an emitter temperature of 600K (1200K) at a distance of 10nm.

V. STATE OF THE ART

By using a much more realistic model of the PV cell Park *et al.* [63] have shown that in a tungsten-InGaSb configuration the efficiency can substantially decrease when making the distance between the emitter and the PV cell smaller. This is due to the fact that the penetration depth of the evanescent waves inside the PV cell becomes very small, because the evanescent waves are exponentially damped on a distance on the order of the distance d in the quasi-static regime. For surface modes it could be shown [64] that the penetration depth scales like $0.25d$ for phonon-polaritonic materials like SiC. As a consequence, for very small distances the heat flux increases dramatically due to the evanescent wave contributions, but it will be dissipated at the interface mainly. Hence, only electron-hole pairs close to the interface of the PV cell will be generated limiting such the conversion efficiency. Park *et al.* report an efficiency of about 20% at a distance of 10nm. Nonetheless, the theoretically predicted generated electric power is still high and has a nominal value of 10^6Wm^2 . Introducing a back reflector to the PV cell could even improve the performance [65]. A detailed discussion of the contribution of the different heat flux channels to the NTPV efficiency can be found in Ref. [60].

Since the work of Park *et al.* the modelling has been further improved and the Moss-Burnstein effect, the impact of series resistance, photon recycling as well as parasitic sub-bandgap absorption and cell cooling has been studied in detail [66–70]. Furthermore, hyperbolic materials have been proposed for replacing the emitter, receiver or the gap region [71–73, 77], because with these materials spectral control, high heat flux levels, and large penetration depths are achievable [74–79]. For example, with the NTPV system in Ref. [77] using a W/SiO₂ hyperbolic emitter and a InAs cell a generated power of 1.78kWm^{-2} is reported at a realistic distance of 100nm.

Despite all those efforts on the theoretical side there is only a single up-to-date experimental study of a NTPV system conducted by Reddy's group [80]. In this pioneer experimental study a Si emitter at temperatures ranging from 525K to 665K is brought in close vicinity of two different TPV cells with band gaps of 0.345eV and 0.303eV. The measured power generated at the high (small) band-gap cell at a nominal distance of 60nm is

40 times larger than at long separation distances. However this power remains relatively small (around 30nW for $T_e = 655$ K) because heat is essentially transferred with frustrated photons. Taking into account the area of circular emitter of radius of $40 \mu\text{m}$ we obtain a power flux of about 6 W m^{-2} and an aspect ratio of 1:3200. Although this value is relatively small and corresponds to an extremely low conversion efficiency ($\approx 0.02\%$) several points can significantly be improved. In particular by scaling up the system size and increasing the emitter temperature 1000 K a 6% conversion efficiency can be expected. Also using an emitter which support a surface wave in the Planck window the radiative heat exchanges between the emitter and the PV cell could surpass by several orders of magnitude the flux exchanged at long separation distances. With these improvements the efficiency of NTPV systems could be even larger than the Schockley-Queisser limit [3].

VI. CONCLUDING REMARKS

In conclusion, the basic concepts to convert the near-field electromagnetic energy confined close to a hot body into electricity have been introduced. We have shown that this near-field technology allows to largely surpass the performances of the classical TPV technology. Despite of its potential several hurdles strongly limit to date the development and the massive deployment of this tech-

nology. On the one hand, near-field heat flux experiments between planar structures in the near-field regime are nowadays possible even down to 25nm distance, but typically not for systems with large areas. Using low conducting spacers to keep the vacuum gap in the system is one possible work around. Another is to replace the vacuum gap by a low conducting but high index or hyperbolic material as recently proposed [73]. Furthermore, it is not trivial to maintain large temperature gradients over very small gaps and the cooling of the cell could further reduce the efficiency of the cell, because the power used to cool the cell has to be taken into account in a global balance. So far, a power output of only 6 W m^{-2} and an efficiency of only 0.02% seems to be a little bit disappointing, but the NTPV technology has a great potential and we are very optimistic that future theoretical and experimental works will improve the efficiencies of NTPV systems step by step to a point where the promised near-field enhancement will be achieved and power outputs of $1 \text{ kW m}^{-2} - 1 \text{ MW m}^{-2}$ and efficiencies around 20-40% are not just the dream of theorists but reality.

Acknowledgments

S.-A. B. acknowledges support from Heisenberg Programme of the Deutsche Forschungsgemeinschaft (DFG, German Research Foundation) under the project No. 404073166.

-
- [1] T.J. Coutts, Renewable and Sustainable Energy Review **3**, 77-184 (1999).
 - [2] A. Lenert, D.M. Bierman, Y. Nam, W.R. Chan, I. Celanovic, M. Soljagic, and E.N. Wang, Nat. Nanotechnol. **9**, 126 (2014).
 - [3] W. Shockley and H. Queisser, J. Appl. Phys. **32**, 510 (1961).
 - [4] M. Laroche, R. Carminati, J.-J. Greffet, J. Appl. Phys. **100**, 063704 (2006).
 - [5] D. Polder and M. van Hove, Phys. Rev. B **4**, 3303 (1971).
 - [6] M. Planck, The theory of heat radiation, (Forgotten Books, Leipzig, 2010).
 - [7] O. Ilic, M. Jablan, J. D. Joannopoulos, I. Celanovic, M. Soljagic, Opt. Expr. **20**, A366 (2012).
 - [8] Energy Information Administration, Household Electricity Reports (2005).
 - [9] G.S. Agarwal, Phys. Rev A **11**, 253 (1975).
 - [10] W. Eckhardt, Z. Phys. B **46**, 85 (1982).
 - [11] I. A. Dorofeyev and E. A. Vinogradov, Phys. Rep. **504**, 75 (2011).
 - [12] A. V. Shchegrov, K. Joulain, R. Carminati, and J.-J. Greffet, Phys. Rev. Lett. **85**, 1548 (2000).
 - [13] K. Joulain and R. Carminati and J.-P. Mulet and J.-J. Greffet, Phys. Rev. B **68**, 245405 (3003).
 - [14] Handbook of Optical Constants of Solids, edited by E. Palik (Academic, New York, 1998).
 - [15] Y De Wilde, F. Formanek, R. Carminati, B. Gralak, P.-A. Lemoine,; K. Joulain, J.-P. Mulet, Y. Chen, and J.-J. Greffet, Nature **444**, 740 (2006).
 - [16] A. Babuty, K. Joulain, P.-O. Chapuis, J.-J. Greffet, Y. D. Wilde, Phys. Rev. Lett. **110**, 146103 (2013).
 - [17] A. Kittel, U. Wischnath, J. Welker, O. Huth, F. Rüting, and S.-A. Biehs, Appl. Phys. Lett. **93**, 193109 (2008).
 - [18] F. Huth, M. Schnell, J. Wittborn, N. Ocelic, and R. Hillenbrand, Nat. Mat. **10**, 352 (2011).
 - [19] A. C. Jones and M. B. Raschke, Nano Lett. **12**, 1475 (2012).
 - [20] Q. Weng, S. Komiyama, L. Yang, Z. An, P. Chen, S.-A. Biehs, Y. Kajihara, W. Lu, Science **360**, 775 (2018).
 - [21] S. Komiyama, J. Appl. Phys. **125**, 010901 (2019).
 - [22] P. Ben-Abdallah, K Joulain, J. Drevillon and G. Domingues, Appl. Phys. Lett. **94**, 15,153117 (2009).
 - [23] R. Messina, J.-P. Hugonin, J.-J. Greffet, F. Marquier, Y. De Wilde, A. Belarouci, L. Frechette, Y. Cordier and P. Ben-Abdallah, Phys. Rev. B **87**, 085421 (2013).
 - [24] E. G. Cravalho and C. L. Tien and R. P. Caren, J. Heat Transf. **89**, 351 (1967).
 - [25] G. A. Domoto and C. L. Tien, J. Heat Transf. **92**, 399 (1970).
 - [26] R. F. Boehm and C. L. Tien, J. Heat Transf. **92**, 405 (1970).
 - [27] R. S. DiMatteo, Masters thesis, Massachusetts Institute of Technology (June 1996).
 - [28] M. D. Whale, Masters thesis, Massachusetts Institute of

- Technology (June 1996).
- [29] J. Pan, *Opt. Lett.* **25**, 369 (2000).
- [30] M.D. Whale and E. G. Cravalho, *IEEE Trans. Energy Convers.* **17**, 130 (2002).
- [31] S. M. Rytov, Y. A. Kravtsov, and V. I. Tatarskii, *Principles of Statistical Radiophysics*, Vol. 3 (Springer, New York, 1989).
- [32] R. S. DiMatteo, P. Greiff, S. L. Finberg, K. A. Young-Waithe, H. K. Choy, M. M. Masaki, and C. G. Fonstad, *Appl. Phys. Lett.* **79**, 1894 (2001).
- [33] P. Ben-Abdallah and K. Joulain, *Phys. Rev. B(R)* **82**, 121419 (2010).
- [34] S.-A. Biehs, E. Rousseau, and J.-J. Greffet, *Phys. Rev. Lett.* **105**, 234301 (2010).
- [35] S.-A. Biehs, P. Ben-Abdallah, and F. S. S. Rosa, *Nanoscale Radiative Heat Transfer and Its Applications, Infrared Radiation*, Vasyil Morozhenko (Ed.), ISBN: 978-953-51-0060-7, InTech (2012).
- [36] A.I. Volokitin and B.N.J. Persson, *Rev. Mod. Phys.* **79**, 1291 (2007).
- [37] J. Pendry, *J. Phys.* **11**, 6621 (1999).
- [38] O. D. Miller, S. G. Johnson, and A. W. Rodriguez, *Phys. Rev. Lett.* **115**, 204302 (2015).
- [39] H. Shim, L. Fan, S. G. Johnson, and O. D. Miller, *Phys. Rev. X* **9**, 011043 (2019).
- [40] W. Jin, R. Messina, A. W. Rodriguez, *Opt. Exp.* **25**, 14746 (2017).
- [41] E. G. Cravalho, G. A. Domoto, C. L. Tien, *Progr. Aeron. Astro.* **21**, 531 (1968).
- [42] C.M Hargreaves, *Phys. Lett. A* **30**, 491 (1969).
- [43] G. A. Domoto and R. F. Boehm and C. L. Tien, *J. Heat Transf.* **92**, 412 (1970).
- [44] R. Ottens, V. Quetschke, S. Wise, A. Alemi, R. Lundock, G. Mueller, D. H. Reitze, D. B. Tanner, B. F. Whiting, preprint arXiv:1103.2389 (2011).
- [45] L. Hu, A. Narayanaswamy, X. Chen, and G. Chen, *Appl. Phys. Lett.* **92**, 133106 (2008).
- [46] T. Kralik and P. Hanzelka and M. Zobac and V. Musilova and T. Fort and M. Horak, *Phys. Rev. Lett.* **109**, 224302 (2012).
- [47] R. St-Gelais, B. Guha, L. Zhu, S. Fan, and M. Lipson, *Nano Lett.* **14**, 6971 (2014).
- [48] B. Song, Y. Ganjeh, S. Sadat, D. Thompson, A. Fiorino, V. Fernández-Hurtado, J. Feist, F. J. Garcia-Vidal, J. C. Cuevas, P. Reddy, E. Meyhofer, *Nat. Nanotech.* **10**, 253 (2015).
- [49] M. Lim, S. S. Lee, and B. J. Lee, *Phys. Rev. B* **91**, 195136 (2015).
- [50] K. Ito, A. Miura, H. Iizuka, and H. Tosiyoshi, *Appl. Phys. Lett.* **106**, 083504 (2015).
- [51] J. I. Watjen, B. Zhao, Z. M. Zhang, *Appl. Phys. Lett.* **109**, 203112 (2016).
- [52] B. Song, D. Thompson, A. Fiorino, Y. Ganjeh, P. Reddy, E. Meyhofer, *Nat. Nanotech.* **11**, 509 (2016)
- [53] M. P. Bernardi, D. Milovich & M. Francoeur, *Nat. Comm.* **7**, 12900 (2016).
- [54] S. Lang, G. Sharma, S. Molesky, P. U. Kränzien, T. Jalas, Z. Jacob, A. Yu. Petrov, and M. Eich, *Sci. Rep.* **7**, 13916 (2017).
- [55] M. Ghashami, H. Geng, T. Kim, N. Iacopino, S. K. Cho, and K. Park, *Phys. Rev. Lett.* **120**, 175901 (2018).
- [56] M. Lim, J. Song, S. S. Lee, B. J. Lee, *Nat. Comm.* **9**, 4302 (2018).
- [57] A. Fiorino, D. Thompson, L. Zhu, B. Song, P. Reddy, and E. Meyhofer, *Nano Lett.* **18**, 3711 (2018).
- [58] A. Narayanaswamy and G. Chen, *Appl.Phys. Lett.* **82**, 3544 (2003).
- [59] A. R. Forouhi and I. Bloomer, *Phys. Rev. B* **38**, 1865 (1988).
- [60] M.P. Bernardi, O. Dupré, E. Blandre, P.-O. Chapuis, R. Vaillon, and M. Francoeur, *Sci. Rep.* **5**, 11626 (2015).
- [61] R. Messina and P. Ben-Abdallah, *Sci. Rep.* **3**, 1383 (2012).
- [62] - V.B. Svetovoy and G. Palasantzas, *Phys. Rev. Applied* **2**, 034006 (2014).
- [63] K. Park, S. Basu, W. P. King, and Z. M. Zhang, *JQSRT* **109**, 305 (2008).
- [64] S. Basu and Z. M. Zhang, *Appl. Phys. Lett.* **95**, 133104 (2009).
- [65] S. Basu, Z. M. Zhang, C. J. Fu, *Int. J. En. Res.* **33**, 1203 (2009).
- [66] K. Chen, P. Santhanam, and S. Fan, *Apl. Phys. Lett.* **107**, 091106 (2015).
- [67] E. Blandre, P.-O. Chapuis, and R. Vaillon, *Sci. Rep.* **7**, 15860 (2017).
- [68] J. DeSutter, R. Vaillon, and M. Francoeur, *Phys. Rev. Applied* **8**, 014030 (2017).
- [69] R. Vaillon, J.-P. Perez, C. Lucchesi, D. Cakiroglu, P.-O. Chapuis, T. Talierno, and E. Tournie, *Opt. Exp.* **27**, 347515 (2019)
- [70] M. S. Mirmoosa and C. R. Simovski, *Phot. Nanostruct. Fundam. Appl.* **13**, 20 (2015).
- [71] I. S. Nefedov and C. Simovski, *Phys. Rev. B* **84**, 195459 (2011).
- [72] C. R. Simovski, S. Maslovski, I. Nefedov, and S. Tretyakov, *Opt. Exp.* **21**, 14988 (2013).
- [73] M. S. Mirmoosa, S.-A. Biehs, and C. R. Simovski, *Phys. Rev. Appl.* **8**, 054020 (2017).
- [74] S.-A. Biehs, M. Tschikin, and P. Ben-Abdallah, *Phys. Rev. Lett.* **109**, 104301 (2012).
- [75] S.-A. Biehs, S. Lang, A. Yu. Petrov, M. Eich, and P. Ben-Abdallah, *Phys. Rev. Lett.* **115**, 174301 (2015).
- [76] B. Liu and S. Shen, *Phys. Rev. B* **87**, 115403 (2013).
- [77] S. Jin, M. Lim, S. S. Lee, and B. J. Lee, *Opt. Exp.* **24**, A635 (2016).
- [78] S. Lang, M. Tschikin, S.-A. Biehs, A. Yu. Petrov, and M. Eich, *Appl. Phys. Lett.* **104**, 121903 (2014).
- [79] M. Tschikin, S.-A. Biehs, P. Ben-Abdallah, S. Lang, A. Yu. Petrov, and M. Eich, *JQSRT* **158**, 17 (2015).
- [80] A. Fiorino, L. Zhu, D. Thompson, R. Mittapally, P. Reddy, and E. Meyhofer, *Nat. Nanotechn.* **13**, 806 (2018).